Acta Pharmaceutica Sinica B 2022;12(2):821−837

Chinese Pharmaceutical Association
Institute of Materia Medica, Chinese Academy of Medical Sciences

Acta Pharmaceutica Sinica B

www.elsevier.com/locate/apsb
www.sciencedirect.com

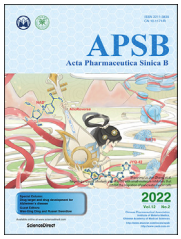

ORIGINAL ARTICLE

miR-7/TGF-β2 axis sustains acidic tumor microenvironment-induced lung cancer metastasis

Tao Su[a,†], Suchao Huang[a,†], Yanmin Zhang[a], Yajuan Guo[a], Shuwei Zhang[a], Jiaji Guan[a], Mingjing Meng[a], Linxin Liu[a], Caiyan Wang[a], Dihua Yu[b], Hiu-Yee Kwan[c], Zhiying Huang[a], Qiuju Huang[a], Elaine Lai-Han Leung[d], Ming Hu[e], Ying Wang[a], Zhongqiu Liu[a,d,*], Linlin Lu[a,d,*]

[a]*Joint Laboratory for Translational Cancer Research of Chinese Medicine of the Ministry of Education of the People's Republic of China, Guangzhou University of Chinese Medicine, Guangzhou 510006, China*
[b]*Department of Molecular and Cellular Oncology, the University of Texas MD Anderson Cancer Center, Houston, TX 77030, USA*
[c]*School of Chinese Medicine, Hong Kong Baptist University, Hong Kong 999077, China*
[d]*State Key Laboratory of Quality Research in Chinese Medicine/Macau Institute for Applied Research in Medicine and Health, Macau University of Science and Technology, Macau (SAR) 999078, China*
[e]*Department of Pharmacological and Pharmaceutical Sciences, University of Houston, Houston, TX 77204, USA*

Received 28 February 2021; received in revised form 23 April 2021; accepted 19 May 2021

KEY WORDS

Acidic tumor microenvironment;
miR-7-5p;
TGF-β2;
Metastasis;

Abstract Acidosis, regardless of hypoxia involvement, is recognized as a chronic and harsh tumor microenvironment (TME) that educates malignant cells to thrive and metastasize. Although overwhelming evidence supports an acidic environment as a driver or ubiquitous hallmark of cancer progression, the unrevealed core mechanisms underlying the direct effect of acidification on tumorigenesis have hindered the discovery of novel therapeutic targets and clinical therapy. Here, chemical-induced and transgenic mouse models for colon, liver and lung cancer were established, respectively. miR-7 and

Abbreviations: AOM/DSS, azoxymethane/dextran sodium sulfate; B[*a*]P, benzopyrene; CA9, carbonic anhydrase IX; DEN, diethylnitrosamine; DSS, dextran sodium sulfate; DAB, diaminobenzidine; DAVID, Database for Annotation, Visualization, and Integrated Discovery; DEPs, differentially expressed proteins; DEGs, differentially expressed genes; GSEA, gene set enrichment analysis; GEMMs, genetically engineered tumor mouse models; IHC, immunohistochemistry; ISH, *in situ* hybridization; KEGG, Kyoto Encyclopedia of Genes and Genomes; LUAD, lung adenocarcinoma; LUSC, lung squamous cell carcinoma; MCT, monocarboxylate transporter; NSCLC, non-small cell lung cancer; NHE, Na^+/H^+ exchanger; PCR, polymerase chain reaction; TMT, tandem mass tagging; TME, tumor microenvironment; V-ATPase, vacuolar ATPase.

*Corresponding authors. Tel.: +86 20 39357902; fax: +86 20 39358071.
E-mail addresses: liuzq@gzucm.edu.cn (Zhongqiu Liu), lllu@gzucm.edu.cn (Linlin Lu).
†These authors made equal contributions to this work.

Peer review under responsibility of Chinese Pharmaceutical Association and Institute of Materia Medica, Chinese Academy of Medical Sciences.

https://doi.org/10.1016/j.apsb.2021.06.009

Lung cancer;
pH;
Invasion

TGF-β2 expressions were examined in clinical tissues (n = 184). RNA-seq, miRNA-seq, proteomics, biosynthesis analyses and functional studies were performed to validate the mechanisms involved in the acidic TME-induced lung cancer metastasis. Our data show that lung cancer is sensitive to the increased acidification of TME, and acidic TME-induced lung cancer metastasis *via* inhibition of miR-7-5p. TGF-β2 is a direct target of miR-7-5p. The reduced expression of miR-7-5p subsequently increases the expression of TGF-β2 which enhances the metastatic potential of the lung cancer. Indeed, overexpression of miR-7-5p reduces the acidic pH-enhanced lung cancer metastasis. Furthermore, the human lung tumor samples also show a reduced miR-7-5p expression but an elevated level of activated TGF-β2; the expressions of both miR-7-5p and TGF-β2 are correlated with patients' survival. We are the first to identify the role of the miR-7/TGF-β2 axis in acidic pH-enhanced lung cancer metastasis. Our study not only delineates how acidification directly affects tumorigenesis, but also suggests miR-7 is a novel reliable biomarker for acidic TME and a novel therapeutic target for non-small cell lung cancer (NSCLC) treatment. Our study opens an avenue to explore the pH-sensitive subcellular components as novel therapeutic targets for cancer treatment.

1. Introduction

During the initiation and evolution of cancer, nascent tumor cells undergo a devastating Darwinian dynamic selection process in the tumor microenvironment (TME), and only TME-adaptive cells survive, thrive, and metastasize[1,2]. Due to the poor blood perfusion, oxygen deprivation, and glycolysis predisposition surrounding the uncontrolled tumor cells, hypoxia and acidosis become the major and ubiquitous characteristics in the TME, which also serve as environmental stressors to educate and reshape tumor cells to acquire phenotypic plasticity and genetic heterogeneity[3,4].

Although acidity is a hallmark of the TME, comparatively less is known about acidosis-induced tumorigenesis. For example, (i) numerous studies have suggested that the acidic microenvironment exerts profound and synergistic effects on carcinogenesis by simultaneously altering various pathological progresses including autophagy[5], immune response[6], angiogenesis[7], proliferation and invasion[8]. Nevertheless, the clinical efficacy of acidosis-targeted treatments varies depending on the cancer type, pathological stage and metastatic phase[9]. These paradoxical phenomena imply that the acidity mediated effects are organ- or cancer-specific. (ii) The predominant phenotype related to acidification in some cancer types remains obscured. According to a reported study, an intracellular pH/extracellular pH (pH_i/pH_e) ratio varying by only 0.1 units may trigger a vast of subsequent biological or pathological processes[9]. In the acidic microenvironment, extracellular H^+ ions accumulate to generate a steep inverse pH gradient with the intercellular alkalinity (the pH_i, particularly in the cytoplasm, can be increased from 7.12 to a maximum of 7.65)[10]. However, many functional targets are localized in subcellular organelles, and whether the pH values in these compartments are different from that in the cytoplasm, and how the independent pH gradients in each subcellular fraction attribute to tumor progression remain unknown. (iii) In addition, although the correlations, either positive or negative, have been found between acidosis and the expression of tumor-related targets, such as ATG5 and LC3II in autophagy[5]; LAMP2 in lysosomes[11]; BCL-2 in apoptosis[12]; IL-2, INF-γ and LDHA in the immune response as well as VEGF, β-catenin, and snail in metastasis[3], the direct effects of acidity on the transcription of these tumor-associated factors are also unclear.

In our current study, we found that miR-7 could be a reliable biomarker for acidosis due to its significant absence in the acidic tumor tissues and its strong correlation with the survival rates of the lung cancer patients. Our findings deepen our understanding on the impact of the acidic microenvironment on tumorigenesis: i) With the identification of the role of the miR-7/TGF-β2 axis in lung carcinogenesis, our data demonstrate that the miRNA synthesis process represents a novel network approach for the discovery of therapeutic targets. ii) Interestingly, our data also found that EGFR-resistant cells (H1975) were responsive to the miR-7-mediated metastasis inhibition, suggesting that miR-7-targeted therapy may serve as an alternative therapeutic approach and brings benefits to those lung cancer patients harbor EGFR gene mutations.

2. Materials and methods

2.1. Chemicals and reagents

Human lung cancer (A549 and H1975), pancreatic cancer (PC3M and DU145), breast cancer (MDA-MB-231 and MCF-7), liver cancer (HepG2 and Huh7), colorectal cancer (HCT-116 and HT29) cells and pulmonary fibroblasts MRC-5 cells were purchased from the American Type Culture Collection (Manassas, VA, USA) and Chinese Academy of Sciences Cell Bank (Shanghai, China), respectively. β-Actin, GAPDH, E-cadherin, N-cadherin and Vimentin primary antibodies were purchased from Santa Cruz Biotechnology (Santa Cruz, CA, USA). TGF-β1, TGF-β2, TGF-β3 were purchased from Abbkine Scientific Co., Ltd. (Bkine, Wuhan, China), and other antibodies were obtained from Cell Signaling Technology Inc. (Beverly, MA, USA). SB431542 was purchased from Selleckchem (USA). miR-7-5p mimics, miR-7-5p inhibitor and their corresponding control were designed and purchased from RiboBio Inc. (Guangzhou, China). Lentiviral miR-7 (Lv-miR-7), lentiviral vector (Lv-NC), si-TGF-β2 and TGF-β2 plasmids were synthesized by GenePharma (Suzhou, China). All materials for cell culture were obtained from Life Technologies Inc. (GIBCO, USA).

2.2. Cell culture and establishment of acidic microenvironment culture conditions

Cells were incubated at 37 °C in a humidified atmosphere of 5% CO_2 in air. To mimic the acidic pH_e environment, RPMI 1640 medium was supplemented with 25 mmol/L each of PIPES (1,4-piperazinediethanesulfonic acid) and HEPES [4-(2-hydroxyethyl)-1-piperazineethanesulfonic acid], and the pH was adjusted to 7.4 or 6.6 as required[13,14]. Cells were cultured in the medium of acidic (pH 6.6) or normal pH (pH 7.4) for 4 days, respectively; for the reverse group, cells were cultured in the medium of pH 6.6 for 96 h and then transferred to culture in the medium of pH 7.4 for another 2 days.

2.3. Invasion assay

Cell invasion was determined by using BD BioCoat™Matrigel™ invasion chamber (24-well plate, 8-mm pore size) (BD Bioscience, San Jose, CA, USA) according to the manufacturer's instructions[15]. Suspensions of 5×10^4 cells in 500 μL of complete medium (pH 7.4) or acidic medium (pH 6.6) were added to the wells and incubated for 24 h at 37 °C in a humidified 5% CO_2 atmosphere. Invaded cells (cells on the lower surface of the membrane) were counted and imaged by a microscope (Leica, Germany). Effects of invasion inhibition or activation on NSCLC cells (A549 and H1975) were examined by using a general TGFβRI inhibitor SB431542, a neutralizing anti-TGF-β2 antibody and the mimic/inhibitor of miR-7-5p, respectively. Nontoxic concentration of 0.5 μg/mL of anti-TGF-β2 antibody or 10 μmol/L of SB431542 was used in this study.

2.4. Real-time quantitative polymerase chain reaction (PCR) analysis

Total mRNA was isolated using Trizol reagent (Invitrogen, USA) and reverse-transcripted into cDNA following the PrimeScript™ RT reagent Kit (TaKaRa, Shiga, Japan). SYBR green real-time PCR amplification and detection were then performed using an ABI 7500 system (Applied Biosystems, Foster City, CA, USA). Relative gene expression was normalized to GAPDH[16].

2.5. Western blot assay

Cell or tissue extracts were prepared, electrophoresed under denaturing conditions. The proteins were transferred onto polyvinyldifluoridine membranes. The membranes were washed in TBS containing 0.05% (*v*/*v*) Tween-20 and incubated over night at 4 °C with corresponding primary antibodies, and then incubated with secondary antibodies. Signals were detected by ECL detection reagents (Amersham Biosciences, USA)[17].

2.6. Flow cytometry analysis

Cells (3×10^5/well) were cultured in the medium of pH 7.4 and pH 6.6 for 4 days, respectively. Then, cells were assessed by Annexin V-propidium iodide kit (BD Biosciences, Auckland, New Zealand). The stained cells were acquired by flow cytometry (BD Biosciences, San Diego, CA, USA) and analyzed by FlowJo v7.6 software.

2.7. miRNAs transfection

miR-7 mimic, miR-7 inhibitor and their corresponding NC (mimics control and inhibitor control) were used in this assay. A549 and H1975 cells were grown to 50% confluence in 6-well plates, and transfected with the miRNAs in Opti-MEM media (Invitrogen) using Lipofectamine™2000 (Invitrogen) according to the manufacturer's instructions. A final concentration of 50 nmol/L miRNA mimic, 50 nmol/L miRNA inhibitor and their corresponding control were used.

2.8. Luciferase reporter assay

A549 cells were seeded in 24-well plates (70%−80% confluence) and then transfected with pmiR-RB-Report™-TGF-β2 (wild-type TGF-β2 3′UTR, WT) and pmiR-RB-Report™-Control (mutant type TGF-β2 3′UTR, MUT) for miR-7 (RiboBio, Guangzhou, China), respectively. Luciferase activity was determined using the dual luciferase assay system (Promega, Wisconsin, USA) after 48 h transfection. Luciferase activity was normalized to *Renilla* luciferase activity[18].

2.9. RNA pull-down assay

RNA pull-down assay was performed using biotin-labeled H19 as a probe, and then examined the expression of miR-7-5p by qRT-PCR. Cell extracts (2 μg) were mixed with biotinylated RNA (100 pmol). Washed streptavidin agarose beads (100 mL) were added to each binding reaction and further incubated at room temperature for 1 h. Total RNAs and controls were also assayed to demonstrate that the detected signals were from RNAs specifically binding to Ago2.

2.10. Imaging of tumor/cancer cells pH

A pH-sensitive fluorescent dye SNARF-1 was used for the pH detection, and the two-photon microscope (Nikon, Japan) was used to detect the fluorescence signal of the SNARF-1 staining in the tumor samples. A fluorescence microscope (Leica, Germany) was used to detect the fluorescence signal of the SNARF-1 staining in A549 cancer cells.

2.11. Animal experiments

Metastatic mouse model: male BALB/c *nu/nu* mice (5−6 weeks) were kept in the animal facility in the SPF animal laboratory [License number: SYXK (GZ) 2019-0144] at International Institute for Translational Chinese Medicine, Guangzhou University of Chinese Medicine (Guangzhou, China). All the animal experiments were approved by the Guangzhou University of Chinese Medicine Animal Care and Use Committee (Guangzhou, China), and conducted according to the ethical standards and national guidelines. Lv-miR-7 A549 cells and Lv-miR-NC A549 cells (2.5×10^6 cells/0.2 mL) were injected into the lateral tail vein of the nude mice, respectively. Mice were randomly divided into 2 groups ($n = 6$): Lv-miR-NC group and Lv-miR-7 group. Each mouse was administrated to drink water freely for 7 consecutive weeks. At the end of the experimental period, mice were sacrificed, lung tissues and tumors of each mouse were dissected.

Chemical-induced lung/liver/colon cancer model. i) Benzopyrene (B[*a*]P)-induced lung cancer mouse model: healthy male A/J mice (18−20 g) were obtained from The Jackson Laboratory. Mice were administered once intraperitoneal injection of B[*a*]P (100 mg/kg). After

one week, they were randomly divided into two groups ($n = 6$), and then gavaged with $NaHCO_3$ (200 mmol/L) or 0.9% NaCl for 45 weeks, respectively. Body weight of each mouse was measured weekly. At the end of the experimental period, mice were sacrificed, lung tissues and tumors of each mouse were dissected. ii) Diethylnitrosamine (DEN)-induced liver cancer mouse model: 4 weeks of male C57BL/6J mice were administered once intraperitoneal injection of DEN (25 mg/kg). After two weeks, they were randomly divided into two groups ($n = 6$), and gavaged with $NaHCO_3$ (200 mmol/L) and 0.9% NaCl for 37 weeks. At the end of the experimental period, mice were sacrificed, liver tissues and tumors of each mouse were dissected. iii) Azoxymethane/dextran sodium sulfate (AOM/DSS)-induced mouse colon cancer model: 4 weeks of female C57BL/6J mice were administered once intraperitoneal injection of AOM (10 mg/kg). After one week, they were randomly divided into two group ($n = 15$), and then treated with 1.5% dextran sodium sulfate (DSS) in their drinking water for one cycle followed by regular water for 14 days. Later, mice were treated with 2% DSS in their drinking water for one cycle followed by regular water for 14 days, and the cycle was repeated twice. Mice in each group were gavaged with $NaHCO_3$ (200 mmol/L) or 0.9% NaCl from 13 to 17 weeks, respectively. At the end of the experimental period, mice were sacrificed, colon tissues and tumors of each mouse were dissected.

Genetically engineered tumor mouse models (GEMMs): i) Transgenic lung cancer mouse model: mice were originally obtained from The Jackson Laboratory and maintained as heterozygotes by breeding with nontransgenic C57BL/6J mice. In mice, homozygosity for the *K-ras*^{LA2} allele is lethal. Heterozygotes (*K-ras*$^{LA2+/-}$) were randomly divided into two groups ($n = 6$), and then gavaged with $NaHCO_3$ (200 mmol/L) or 0.9% NaCl for 120 days, respectively. At the end of the experimental period, mice were sacrificed, lung tissues and tumors of each mouse were dissected. ii) Transgenic liver cancer mouse model: *Myc-OV* mice were purchased from Shanghai Model Organisms Center (Shanghai, China). All Myc wild-type and *Myc-OV* mice were generated from Myc heterozygous mice (C57BL/6J). Four weeks of *Myc-OV* mice were randomly divided into two groups ($n = 6$), and then gavaged with $NaHCO_3$ (200 mmol/L) or 0.9% NaCl for 6 weeks, respectively. At the end of the experimental period, mice were sacrificed, liver tissues and tumors of each mouse were dissected. iii) Transgenic colon cancer mouse model: mice were originally obtained from The Jackson Laboratory and maintained as heterozygotes by breeding with nonmutated C57BL/6J mice. In mice, homozygosity for the *APC*^{min} allele is lethal. Four weeks of *APC*$^{min/+}$ mice were randomly divided into two groups ($n = 6$), and then gavaged with $NaHCO_3$ (200 mmol/L) or 0.9% NaCl for 9 weeks, respectively. Body weight was measured weekly. At the end of the experimental period, mice were sacrificed, liver tissues and tumors of each mouse were dissected.

2.12. Patient tissue specimens

A LUAD tissue microarray (TMA, HLugA180Su06; Shanghai Outdo Biotech) and a LUSC tissue microarray (TMA, HLugS180Su01; Shanghai Outdo Biotech) were obtained from the National Engineering Center for Biochip in Shanghai. The TMA (HLugA180Su06) was constructed with 94 paired formalin-fixed, paraffin-embedded LUAD tissues and their corresponding adjacent normal tissues. The TMA (HLugS180Su01) was constructed with 90 paired formalin-fixed, paraffin-embedded LUSC tissues and their corresponding adjacent normal tissues. Patients were followed up for 8−10 years. Patients with diagnosed relapse as well as those who received preoperative radiation, chemotherapy or biotherapy were excluded. Demographic and clinical data were obtained from the patients' medical records. Detailed clinicopathological information was listed in Supporting Information Tables S1 and S2.

2.13. Immunohistochemistry (IHC) staining

Tumor specimens from nude mice were fixed in 4% paraformaldehyde and were then embedded in paraffin. Samples were then incubated at 4 °C overnight with primary antibodies against TGF-β2, and then treated with secondary antibody for 30 min, stained with diaminobenzidine (DAB) until brown granules appeared. Sections were blindly evaluated *via* two pathologists with light microscopy.

2.14. In situ hybridization (ISH)

All the paraffin sections were examined *via* locked nucleic acid (LNA)-based ISH using digoxigenin (DIG)-labeled miRCURY miRNA probes (Exiqon, Vedbaek, Denmark). The protocol for miRNA detection was as previously described, and staining was visualized by the addition of BM-Purple AP substrate (Roche) according to the manufacturer's instructions[15].

2.15. Expression data analysis in databases

miRNAs were predicted by miRDB (http://mirdb.org/), StarBase (http://starbase.sysu.edu.cn) and TargetScan 7 (http://www.targetscan.org) databases. All expression profiling data of the miRNAs and mRNAs analyzed in this study were downloaded from the Gene Expression Omnibus (GEO, http://www.ncbi.nlm.nih.gov/geo/) and The Cancer Genome Atlas (TCGA, http://cancergenome.nih.gov/) databases.

2.16. RNA-seq analysis

Cells were collected, and total RNA for RNA-seq was isolated using TRIzol (Invitrogen, CA, USA). RNA quantification and integrity were measured by BioAnalyzer 2100 (Agilent, CA, USA). Oligo (dT) magnetic beads (Invitrogen, CA, USA) were used to enrich mRNA. Then, mRNA was fragmented, reverse transcribed to cDNA and amplified with Phusion High Fidelity DNA polymerase as previously reported[19]. Each PCR product was single-end (50 bps) sequenced on a BGISEQ-500 sequencer (BGI, Shenzhen, China). Gene expression levels were quantified by RSEM software[20]. False discovery rate (FDR, Benjamini Hochberg method) of $\leq$0.001 and cut-off of $\log_2$ fold change $\geq$1 as the threshold was used to assess the significance of differential gene expression between control-4D *vs.* acid-4D, and control-30D *vs.* acid-30D, respectively. The Database for Annotation, Visualization, and Integrated Discovery (DAVID) online tool was used for KEGG pathway enrichment analysis of the selected DEGs[21]. GSEA was used to evaluate the related pathways affected by leading edge genes[22].

2.17. miRNA-seq analysis

miRNA expression profiling was performed on 100 ng of RNA isolated from pH 7.4 medium- and pH 6.6 medium-treated A549 cells. Total RNA was labeled with Cy3 and amplified using Low Input Quick Amp Labeling Kit according to the manufacturer's instructions. After RNA purification, labeled RNA was hybridized to Agilent 8 × 15 K Human miRNA Microarray

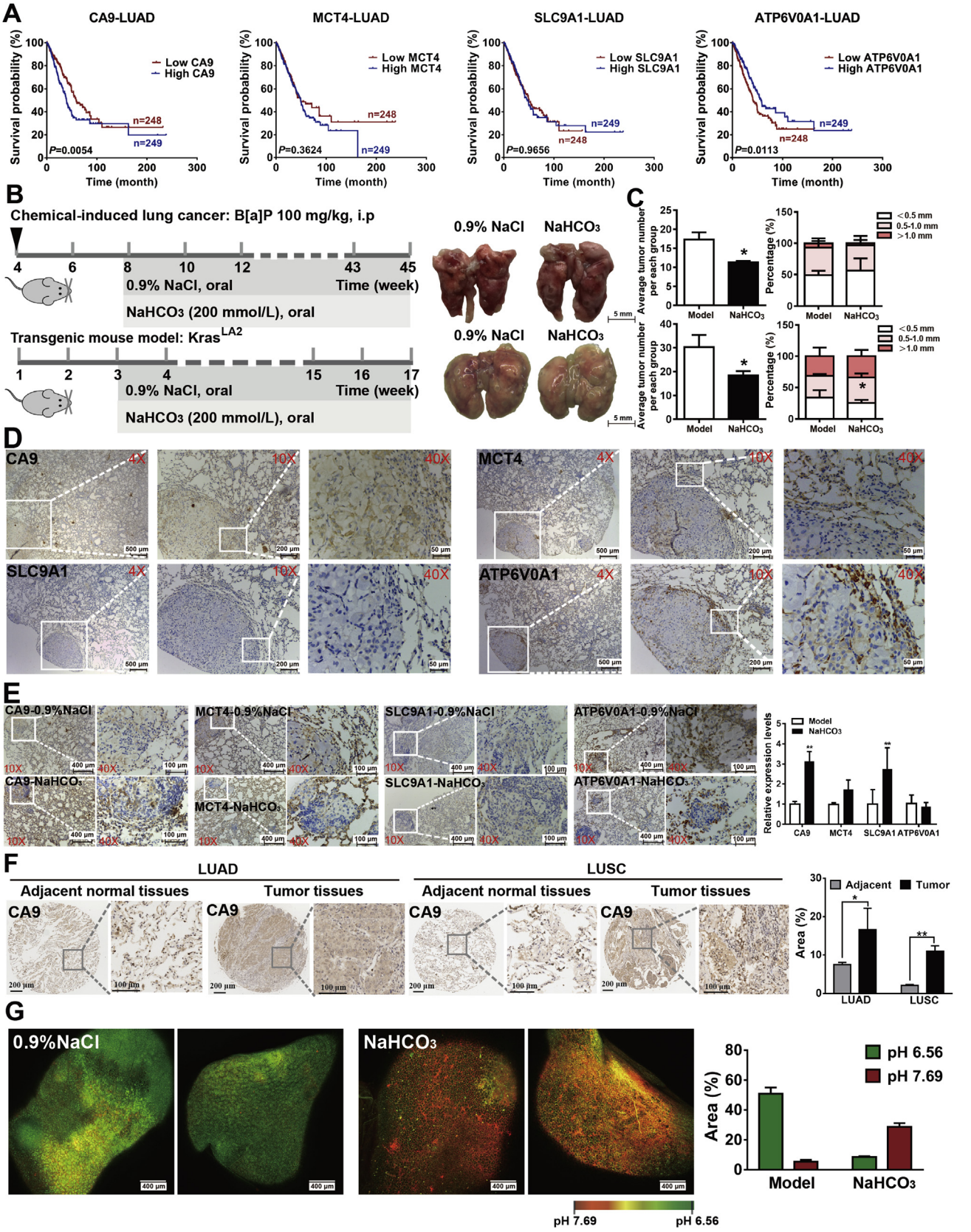

Figure 1 The lung TME is acidic. (A) Survival curves of CA9, MCT4, SLC9A1, ATP6V0A1 in lung cancer ($n = 497$). (B) Timeline and representative tumor images of the [B(*a*)P]-induced and transgenic animal models for lung cancer. (C) Tumor number and tumor size of the mice. (D) IHC results for CA9, MCT4, SLC9A1 and ATP6V0A1 in lung tumor tissues of mice. (E) IHC results for CA9, MCT4, SLC9A1 and ATP6V0A1 in lung tumor tissues of 0.9% NaCl- and $NaHCO_3$-treated mice, respectively. (F) IHC results for CA9 in tumor tissues and adjacent normal tissues of clinical LUAD and LUSC patients. (G) The pH of lung tumor was measured by using an A1R MP two-photon confocal microscope (Nikon, Japan, 4×). For the *in vivo* study, data are presented as mean ± SD, $n = 6$, $^*P < 0.05$ *vs.* model group.

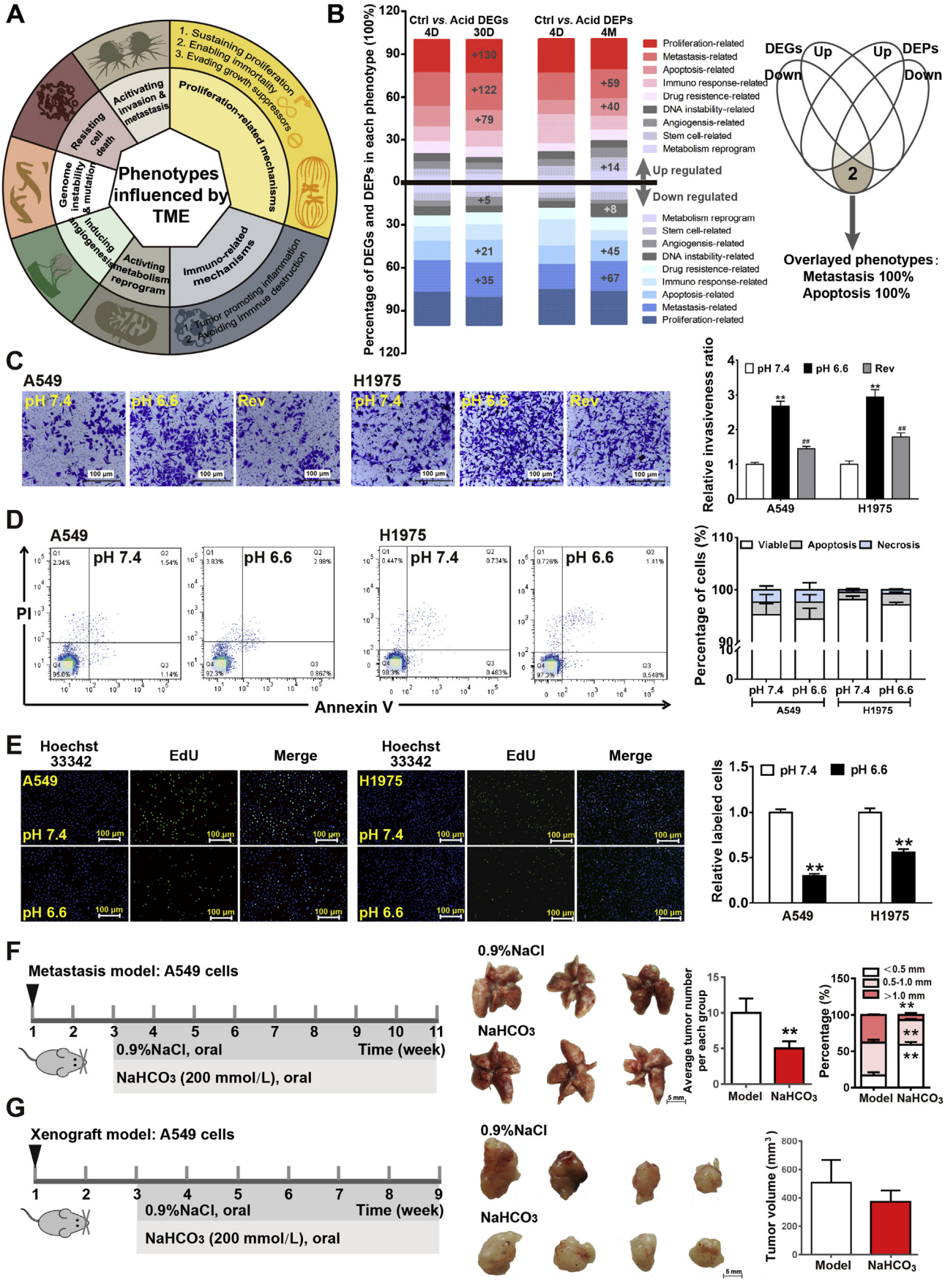
A
Phenotypes influenced by TME
Proliferation-related mechanisms
1. Sustaining proliferation
2. Enabling immortality
3. Evading growth suppressors
Immuno-related mechanisms
1. Tumor promoting inflammation
2. Avoiding immune destruction
Activting metabolism reprogram
Inducing angiogenesis
Genome instability & mutation
Resisting cell death
Acitivating invasion & metastasis
B
Ctrl vs. Acid DEGs 4D 30D
Ctrl vs. Acid DEPs 4D 4M
Percentage of DEGs and DEPs in each phenotype (100%)
Proliferation-related
Metastasis-related
Apoptosis-related
Immuno response-related
Drug resistence-related
DNA instability-related
Angiogensis-related
Stem cell-related
Metabolism reprogram
Up regulated
Down regulated
+130
+122
+79
+5
+21
+35
+59
+40
+14
+8
+45
+67
DEGs Up Down
DEPs Up Down
2
Overlayed phenotypes:
Metastasis 100%
Apoptosis 100%
C
A549
H1975
pH 7.4
pH 6.6
Rev
100 μm
Relative invasiveness ratio
A549
H1975
D
A549
H1975
PI
Annexin V
Q1 2.34%
Q2 1.54%
Q4 95.0%
Q3 1.14%
Q1 3.83%
Q2 2.98%
Q4 92.3%
Q3 0.867%
Q1 0.447%
Q2 0.734%
Q4 98.3%
Q3 0.463%
Q1 0.728%
Q2 1.41%
Q4 97.3%
Q3 0.549%
Viable
Apoptosis
Necrosis
Percentage of cells (%)
E
Hoechst 33342
EdU
Merge
A549
H1975
pH 7.4
pH 6.6
Relative labeled cells
F
Metastasis model: A549 cells
1 2 3 4 5 6 7 8 9 10 11
0.9%NaCl, oral
Time (week)
NaHCO3 (200 mmol/L), oral
0.9%NaCl
NaHCO3
5 mm
Average tumor number per each group
Model
NaHCO3
<0.5 mm
0.5-1.0 mm
>1.0 mm
Percentage (%)
G
Xenograft model: A549 cells
1 2 3 4 5 6 7 8 9
0.9%NaCl, oral
Time (week)
NaHCO3 (200 mmol/L), oral
0.9%NaCl
NaHCO3
5 mm
Tumor volume (mm3)
Model
NaHCO3

Release 12.0. slides (Agilent Technologies) according to the manufacturer's instructions. Small RNA sequencing was performed at BGI using Illumina Small RNA Sequencing Platform. For library preparation, a TruSeq Small RNA library preparation kit (Illumina, San Diego, CA, USA) was used. Sequencing was performed with SE50 runs in an Illumina HiSeq 2000 system, and 10-Mb clean reads were analyzed followed by routine algorithms (BGI Tech Solutions, Shenzhen, China).

2.18. *Tandem mass tagging (TMT) proteomic analysis*

Cells cultured in the medium of pH 7.4 and pH 6.6 for 4 days or 4 months were collected for the proteomic analysis, respectively. The primary experimental procedures for TMT proteomic analysis included protein preparation, trypsin digestion, TMT labeling, HPLC fractionation, LC−MS/MS analysis and data analysis. The TMT proteomics analysis in our research was supported by Jingjie PTM BioLabs[23].

2.19. *Statistical analysis*

All statistical analyses were conducted using GraphPad Prism 7. Two-tailed unpaired *t*-tests were used when comparing two groups. When comparing three groups, ANOVA tests were used with Tukey's multiple comparisons tests to calculate adjusted *P* values. *P* value of 0.05 or lower was considered statistically significant. Survival analysis of the patients was compared by the Kaplan−Meier method and the log-rank (Mantel−Cox) test.

3. Results

3.1. *The lung TME is acidic*

Solid tumors are invariably more acidic than their normal tissue counterparts[24]. The acidic pH_e environment is a distinctive feature of tumor, which is finely tuned by different ion/proton pumps, such as carbonic anhydrase IX (CA9), monocarboxylate transporter (MCT), Na^+/H^+ exchanger (NHE) and vacuolar ATPase (V-ATPase). The expressions and activities of these ion/protein pumps are often enhanced in human tumor[25]. For example, high expression of CA9 is reported to be associated with poor prognosis[26−28], genetic silencing of CA9 leads to a 85% reduction in tumor growth[9], suggesting that CA9 is a critical pro-survival pH-regulating enzyme in the tumor. Among lung, liver, breast, colon and prostate cancers, which have high incidences and low survival rates, high expression of CA9 is directly correlated with the low survival rate of lung cancer (Fig. 1A, $P = 0.0054$) and liver cancer (Supporting Information Fig. S1A, $P = 0.0009$) as revealed in our survival analysis with TCGA database.

Increasing evidence suggests that $NaHCO_3$ neutralizes the acidic pH in TME[29]. Here, lung, liver and colon cancer which are known to be strongly affected by the pH environment in TME were chosen to test the ability of $NaHCO_3$ in neutralizing the acidic pH *in vivo*. Fig. 1B, Fig. S1B and S1D show the timeline of the chemical-induced and transgenic mouse models for colon, liver, and lung cancer, respectively. Administration of $NaHCO_3$ with oral gavage significantly reduced the number and size of lung tumors (Fig. 1C) but not colon tumors (Fig. S1E). Between the two liver cancer mouse models, $NaHCO_3$ administration reduced the tumor numbers in the chemical-induced model but showed no significant effect on the transgenic mouse model (Fig. S1C). The treatment did not cause animal death in all the groups. More importantly, CA9 expression was higher in the tumor tissues than in the adjacent normal tissues (Fig. 1D), the high expression of CA9 was significantly reduced by $NaHCO_3$ treatment (Fig. 1E).

We next examined the CA9 expression in clinical lung tissues. An array comprising 94 paraffin-embedded primary lung adenocarcinoma (LUAD) specimens and their corresponding normal specimens, and another array with 90 paraffin-embedded primary lung squamous cell carcinoma (LUSC) specimens and their corresponding normal specimens were used. The expression levels of CA9 were higher in both LUAD and LUSC than their corresponding adjacent normal tissues (Fig. 1F). Moreover, the pH value of the samples was below 7.0 in the 0.9% NaCl-treated group but was above 7.0 in the $NaHCO_3$-treated group (Fig. 1G). Taken together, our data clearly demonstrate that the TME, particularly in the lung cancer is acidic, which confers the cancer a characteristic that can be served as a therapeutic target.

3.2. *Acidic TME increases the metastatic potential of lung cancer both in vitro and in vivo*

Studies suggest that the increased acidification of TME not only enhances cancer growth[30], metabolism[31] but also metastasis[29] (Fig. 2A). To explore the underlying mechanism of action, we adopted a well-known method to mimic the acidic TME *in vitro* by adjusting the pH of the medium[13,31]. We first ascertain whether the acidic environment in this model was stable and had effects on the cancer cells by examining the mRNA and protein levels of the proton pump-related markers in A549 cells. After cultured in medium of pH 6.6 for 4 days, cancer cells showed elevated protein and mRNA levels of *CA9*, *MCT4*, *NHE1* and *ATP6V0A1* when compared to those cultured in medium of pH 7.4 (Supporting Information Fig. S2A and S2B), suggesting that the acidified medium mimics the acidic condition in the TME. Nevertheless, the mRNA levels of *SLC9A1* and *ATP6V0A1* were not affected or time-dependently affected by the acidified medium. Therefore, identification of markers that are sensitive to the acidic environment is urgently needed.

Figure 2 Acidic pHe promotes lung cancer cell invasiveness and lung tumor metastasis. (A) Phenotypes influenced by acidic TME. (B) RNA-seq and proteomic analyses. RNA-seq analysis was performed after A549 cells cultured in the medium of pH 7.4 and pH 6.6 for 4 days or 30 days, respectively; proteomic analysis was performed after A549 cells cultured in the medium of pH 7.4 and pH 6.6 for 4 days or 4 months, respectively. Overlapping phenotypes of DEGs and DEPs were metastasis and apoptosis. (C) A549 cells invasion was assessed by using Transwell assay. Cells were cultured in the medium of pH 7.4, pH 6.6 and reverse condition. (D) A549 cells apoptosis was assessed by using Annexin V/PI double staining. (E) A549 cells proliferation was assessed by using an EdU assay. (F) Timeline and representative tumor images of lung metastatic mouse model. Tumor number and tumor size were also shown. (G) Timeline and representative tumor images of lung xenograft mouse model. Tumor volume were also shown. For the *in vivo* study, data are presented as mean ± SD, $n = 6$, $^{**}P < 0.01$ *vs.* model group; For the *in vitro* study, data are shown as mean ± SD from three independent experiments; $^{**}P < 0.01$ *vs.* cells cultured in the medium of pH 7.4, $^{\#\#}P < 0.01$ *vs.* cells cultured in the medium of pH 6.6.

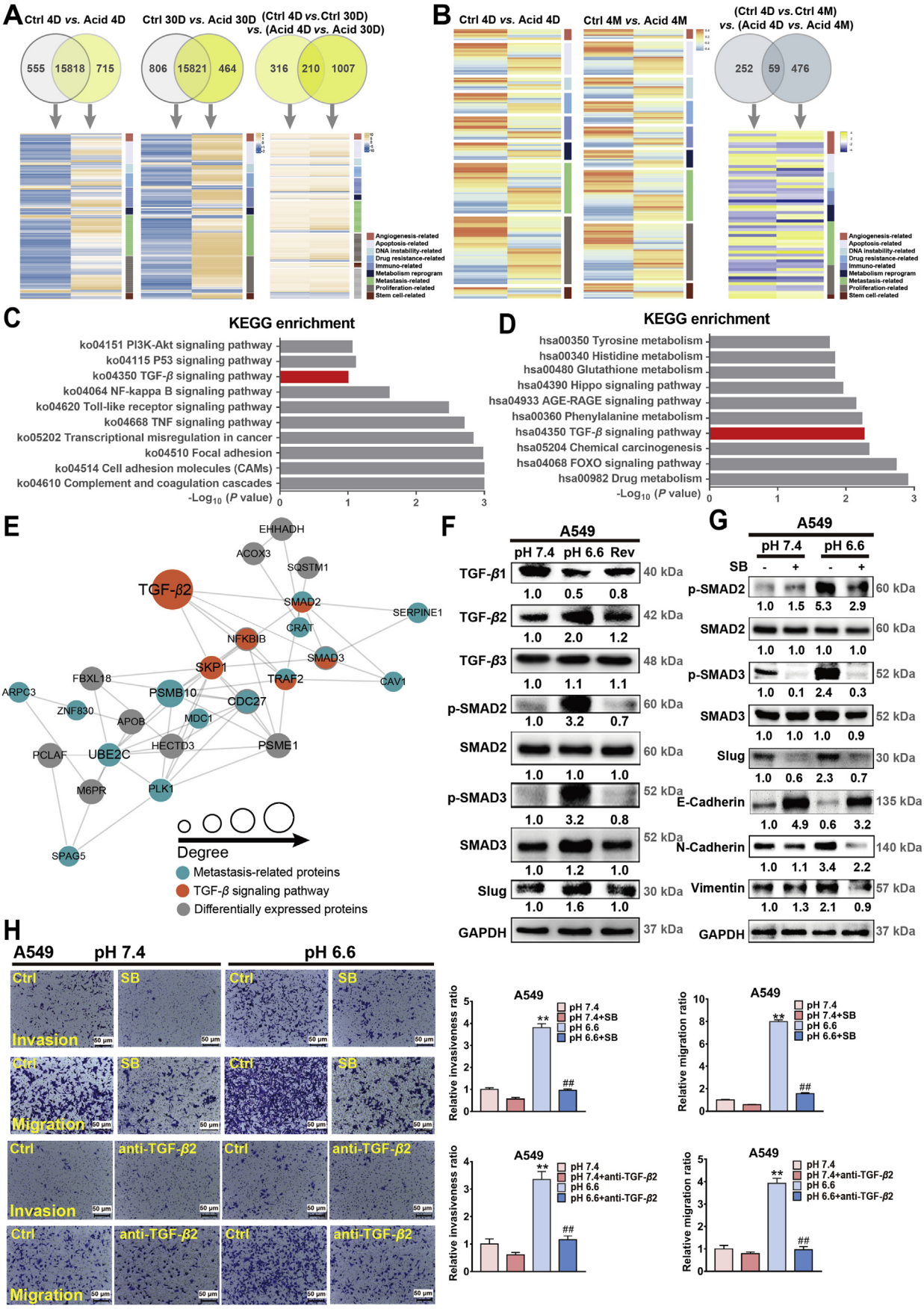
A
Ctrl 4D vs. Acid 4D
555 15818 715
Ctrl 30D vs. Acid 30D
806 15821 464
(Ctrl 4D vs.Ctrl 30D) vs. (Acid 4D vs. Acid 30D)
316 210 1007
B
Ctrl 4D vs. Acid 4D
Ctrl 4M vs. Acid 4M
(Ctrl 4D vs. Ctrl 4M) vs. (Acid 4D vs. Acid 4M)
252 59 476
Angiogenesis-related
Apoptosis-related
DNA instability-related
Drug resistance-related
Immuno-related
Metabolism reprogram
Metastasis-related
Proliferation-related
Stem cell-related
C
KEGG enrichment
ko04151 PI3K-Akt signaling pathway
ko04115 P53 signaling pathway
ko04350 TGF-β signaling pathway
ko04064 NF-kappa B signaling pathway
ko04620 Toll-like receptor signaling pathway
ko04668 TNF signaling pathway
ko05202 Transcriptional misregulation in cancer
ko04510 Focal adhesion
ko04514 Cell adhesion molecules (CAMs)
ko04610 Complement and coagulation cascades
-Log10 (P value)
D
KEGG enrichment
hsa00350 Tyrosine metabolism
hsa00340 Histidine metabolism
hsa00480 Glutathione metabolism
hsa04390 Hippo signaling pathway
hsa04933 AGE-RAGE signaling pathway
hsa00360 Phenylalanine metabolism
hsa04350 TGF-β signaling pathway
hsa05204 Chemical carcinogenesis
hsa04068 FOXO signaling pathway
hsa00982 Drug metabolism
-Log10 (P value)
E
EHHADH
ACOX3
SQSTM1
TGF-β2
SMAD2
SERPINE1
CRAT
NFKBIB
SMAD3
SKP1
FBXL18
TRAF2
CAV1
ARPC3
PSMB10
CDC27
ZNF830
APOB
MDC1
PCLAF
UBE2C
HECTD3
PSME1
M6PR
PLK1
SPAG5
Degree
Metastasis-related proteins
TGF-β signaling pathway
Differentially expressed proteins
F
A549
pH 7.4 pH 6.6 Rev
TGF-β1 40 kDa 1.0 0.5 0.8
TGF-β2 42 kDa 1.0 2.0 1.2
TGF-β3 48 kDa 1.0 1.1 1.1
p-SMAD2 60 kDa 1.0 3.2 0.7
SMAD2 60 kDa 1.0 1.0 1.0
p-SMAD3 52 kDa 1.0 3.2 0.8
SMAD3 52 kDa 1.0 1.2 1.0
Slug 30 kDa 1.0 1.6 1.0
GAPDH 37 kDa
G
A549
pH 7.4 pH 6.6
SB - + - +
p-SMAD2 60 kDa 1.0 1.5 5.3 2.9
SMAD2 60 kDa 1.0 1.0 1.0 1.0
p-SMAD3 52 kDa 1.0 0.1 2.4 0.3
SMAD3 52 kDa 1.0 1.0 1.0 0.9
Slug 30 kDa 1.0 0.6 2.3 0.7
E-Cadherin 135 kDa 1.0 4.9 0.6 3.2
N-Cadherin 140 kDa 1.0 1.1 3.4 2.2
Vimentin 57 kDa 1.0 1.3 2.1 0.9
GAPDH 37 kDa
H
A549
pH 7.4
pH 6.6
Ctrl
SB
Invasion
Migration
anti-TGF-β2
50 μm
A549
pH 7.4
pH 7.4+SB
pH 6.6
pH 6.6+SB
Relative invasiveness ratio
Relative migration ratio
pH 7.4+anti-TGF-β2
pH 6.6+anti-TGF-β2
**
##

To identify the marker or the phenotype in the lung cancer that is most sensitive to the acidic environment, we performed RNA sequencing (RNA-seq) analyses and proteomics analyses with the cells in this model. For the RNA-seq, A549 cells were cultured in medium of pH 7.4 and pH 6.6 for 4 days and 1 month, respectively. For the proteomics, A549 cells were cultured in medium of pH 7.4 and pH 6.6 for 4 days and 4 months, respectively. The differentially expressed genes (DEGs) and differentially expressed proteins (DEPs) between these cell groups were compared at different time points. As shown in Fig. 2B, for the up-regulated DEGs, the top 3 cell phenotype-terms enriched in DEGs were cell proliferation, metastasis and apoptosis, with 130, 122, and 79 DEGs highlighted, respectively. For the down-regulated DEGs, the top 3 cell phenotype-terms enriched in DEGs were cell metastasis, apoptosis and angiogenesis, with 35, 21, and 5 DEGs highlighted, respectively. Regarding the up-regulated DEPs, the top 3 cell phenotype-terms enriched in DEPs were cell metastasis, apoptosis and metabolism, with 59, 40, and 14 DEPs highlighted, respectively. For the down-regulated DEPs, the top 3 cell phenotype-terms enriched in DEPs were cell metastasis, apoptosis and DNA instability, with 67, 45, and 8 DEPs highlighted, respectively. Hence, both the RNA-seq and proteomics analysis suggest that the top 2 phenotypes that are most sensitive to acidic environment are metastasis and apoptosis, followed by proliferation and metabolism which are the top 2 partially overlapping phenotypes in these two analyses.

Next, we investigated whether metastasis, apoptosis, proliferation and metabolism were sensitive to the acidic environment with different *in vitro* models. Our data show that an acidic environment significantly enhanced the invasiveness of NSCLC cells (A549 and H1975) (Fig. 2C); however, it did not affect cell apoptosis (Fig. 2D). In addition, the acidic environment inhibited cell proliferation (Fig. 2E), and enhanced the lipid metabolism of H1975 cells but not A549 cells (Fig. S2C). Indeed, in animal models, our data also show that acidic TME significantly enhanced lung tumor metastasis (Fig. 2F) but did not affect the tumor growth (Fig. 2G), which is in consistent with our *in vitro* results.

We also investigated the effects of the acidic environment on invasion with the other four types of solid tumors that have high incidences and low survival rates. Indeed, breast cancer cells (MDA-MB-231) and prostate cancer cells (PC-3M) cultured in medium of pH of 6.6 also had enhanced invasiveness (Fig. S2D). However, among the 5 cancer types, the stimulatory effect of the acidic environment (pH 6.6) on invasion is most prominent in lung cancer. Interestingly, the reversed pH condition significantly reduced the stimulatory effects of the acidic medium (pH 6.6) on both A549 and H1975 cells invasion (Fig. 2C). Taken together, these results clearly demonstrate that metastasis is the phenotype that is most sensitive to the acidic TME in the lung cancer.

The enhanced invasiveness of these lung cancer cells under the acidic environment was coupled with morphological changes. It was obvious that cells cultured in acidic medium (pH 6.6) underwent a marked EMT-like transformation, as evidenced by morphological alteration from an epithelial (polygonal cells arranged in cobblestone-like sheets) to a more mesenchymal (loose cell contacts) morphology with cells that scattered from clusters and acquired an elongated, fusiform morphology with dendritic processes phenotype. More importantly, reversing the acidic condition significantly restored the cell morphology to a phenotype that was similar to those cultured in medium with pH 7.4 (Fig. S2E). Further studies showed that the acidic environment significantly enhanced the mRNA expressions of the most critical metastasis-related markers, such as snail and *Zeb1* (Fig. S2F); and significantly inhibited the protein levels of E-cadherin and increased the protein levels of N-cadherin and Vimentin in both A549 and H1975 cells (Fig. S2G).

3.3. *TGF-β2/SMAD signaling is involved in acidic pH_e-induced lung cancer metastasis*

To explore the mechanisms of action underlying the acidic pH_e-enhanced metastasis, we further analyzed the RNA-seq and proteomics results. In RNA-seq, 210 overlapping DEGs were highlighted after A549 cells were cultured in medium of pH 6.6 for 4 days or 1 month (Fig. 3A). In proteomics, 59 overlapping DEPs were highlighted after A549 cells were cultured in medium of pH 6.6 for 4 days or 4 months (Fig. 3B). Gene set enrichment analysis (GSEA) shows that the overlapping DEGs were clustered into the metastatic phenotype (Supporting Information Fig. S3A). More importantly, the Kyoto Encyclopedia of Genes and Genomes (KEGG) enrichment analysis results clearly indicated that both the overlapping DEGs and DEPs were clustered into the TGF-β2 signaling pathway (Fig. 3C and D). The interactions between TGF-β2 and other metastasis-related proteins are shown in Fig. 3E.

We next validated whether TGF-β2 signaling pathway was involved in the acidic pH-induced lung cancer metastasis. In mammals, TGF-β exists in three isoforms, they are TGF-β1, TGF-β2 and TGF-β3[32]. Here, we found that the acidic environment (pH 6.6) significantly increased the protein and mRNA levels of *TGF-β2* but not the *TGF-β1* and *TGF-β3* isoforms. Moreover, reversal of the acidic environment reduced the enhanced TGF-β2 in A549 (Fig. 3F) and H1975 (Fig. S3B) cells. TGF-β signaling is involved in both SMAD-dependent and SMAD-independent pathways (*e.g.*, PI3K/AKT, MAPK, STAT3 signaling pathways, etc)[33]. The TGF-

Figure 3 Acidic pHe-induces EMT *via* activation of the TGF-β2/SMAD signaling pathway. (A) Venn diagrams depicting the overlapping DEGs in A549 cells after cultured in the medium of pH 7.4 and pH 6.6 for 4 days or 30 days, respectively. Heatmaps show the overlapping DEGs with different cell phenotypes. (B) Venn diagrams depicting the overlapping DEPs in A549 cells after cultured in the medium of pH 7.4 and pH 6.6 for 4 days or 4 months, respectively. Heatmaps show the overlapping DEPs with different cell phenotypes. (C) Pathway enrichment were identified by KEGG analysis of DEGs. (D) Pathway enrichment identified by KEGG analysis of DEPs. (E) Interaction among different proteins in the metastatic phenotype. (F) The protein levels of TGF-β1, TGF-β2, TGF-β3, p-SMAD2, SMAD2, p-SMAD3, SMAD3 and Slug in A549 cells after cultured in the medium of pH 7.4, pH 6.6 and reverse condition were measured by using Western blot analysis. (G) The protein levels of p-SMAD2, SMAD2, p-SMAD3, SMAD3, Slug, E-cadherin, N-cadherin and Vimentin in A549 cells after cultured in the medium of pH 7.4 and pH 6.6 in the presence/absence of SB-431542 were measured by using Western blot analysis. (H) Representative images of invaded or migrated A549 cells after cultured in the medium of pH 7.4 and pH 6.6 in the presence/absence of SB-431542 or an anti-TGF-β2 antibody. For the *in vitro* study, data are shown as mean ± SD from three independent experiments. $^{**}P < 0.01$ *vs.* cells cultured in the medium of pH 7.4, $^{\#\#}P < 0.01$ *vs.* cells cultured in the medium of pH 6.6.

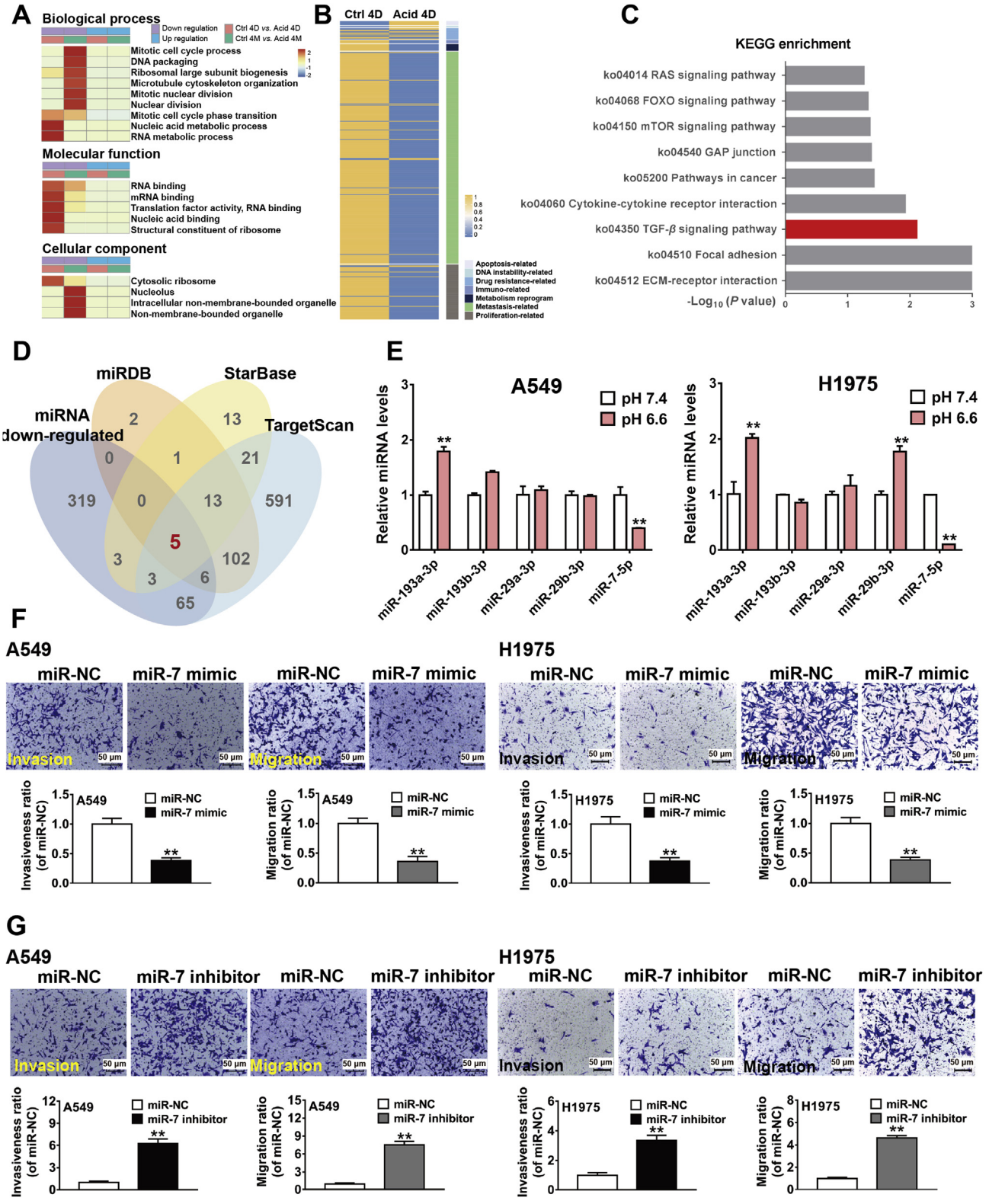

Figure 4 Acidic pHe-induces EMT *via* downregulation of miR-7-5p in both A549 and H1975 cells. (A) Heatmaps showing the changes in biological processes, molecular functions and cellular components between cells cultured in the medium of pH 7.4 and pH 6.6 for 4 days or 4 months, respectively. (B) Heatmaps of the miRNA-seq data showing the different cell phenotypes. (C) Pathway enrichment were identified by KEGG analysis of differentially expressed miRNAs. (D) Venn diagram depicting the overlapping TGF-β2-related miRNAs identified in three databases and the down-regulated miRNAs that from the miRNA-Seq. Five overlapping miRNAs were shown. (E) The expressions of five potential miRNAs in NSCLC cells (A549 and H1975) after cultured in the medium of pH 7.4 and pH 6.6 were determined by using qRT-PCR analysis. $^{**}P < 0.01$ *vs.* cells cultured in the medium of pH 7.4. (F) Representative images of the migrated and invade cells after treating

β/SMAD signaling pathway is a classical pathway that is activated *via* the phosphorylation of SMAD2/SMAD3[33]. Our data show that the acidic pH_e significantly increased the phosphorylation of SMAD2 and SMAD3. Reversal of the acidic environment reduced the acidic pH-enhanced mRNA expressions of *SMAD3* and *SLUG* (Fig. S3C), as well as the protein expressions of phosphorylated SMAD2, SMAD3 and slug in A549 (Fig. 3F) and H1975 (Fig. S3B) cells. Interestingly, the SMAD-independent pathways, such as AKT, MAPK, and STAT3 signaling pathways were not affected by the acidic environment (Fig. S3E). Collectively, these results suggest that TGF-β2/SMAD signaling is involved in acidic pH-induced lung cancer metastasis.

To further validate the involvement of the TGF-β2/SMAD signaling pathway, we examined whether inhibition of the TGF-β2/SMAD signaling pathway ameliorated the stimulatory effects of the acidic pH on lung cancer metastasis. We treated the cells with SB431542, a commonly used TGFβ type I receptor (TGFβRI) inhibitor, under the acidic environment. As expected, inhibition of the signaling pathway reversed the acidic pH_e-enhanced expressions of SMAD2, SMAD3, Slug, N-cadherin and Vimentin as shown in A549 and H1975 cells; the SB431542 treatment also diminished the elevated E-cadherin protein expressions in these cells (Fig. 3G and Fig. S3D). More importantly, SB431542 treatment significantly reduced the migration and invasion of the NSCLC cells (A549 and H1975) that were cultured in the medium of either pH 7.4 or pH 6.6. Furthermore, similar results were observed after TGF-β2 neutralizing antibody treatment (5 μg/mL of anti-TGF-β2 antibody) (Fig. 3H and Fig. S3F), suggesting that activation of TGF-β2/SMAD signaling contributes to the acidic pH_e-enhanced EMT and metastasis in NSCLC (A549 and H1975) cells, which can be reversed by inhibiting TGF-β2.

3.4. *miR-7-5p is a potential target that regulated by acidic TME*

Our proteomic analysis showed that the acidic environment mainly affected RNA metabolic processes, RNA binding, nucleic acid binding and signal transduction (Fig. 4A). In response to stimuli, the dysregulated miRNAs may affect many biological processes, molecular functions and cellular signaling components of the cancer cells. Hence, we compared the miRNA-Seq data (miRNA expression profiles) of the A549 cells cultured in the acidic medium (pH 6.6) for either 4 days or 1 month *vs.* those cultured in normal medium (pH 7.4). The data showed that a total of 152 genes that showed differential expressions were overlapped in the A549 cells that were cultured in the acidic medium for 4 days and 1 month (Supporting Information Fig. S4A). Importantly, Fig. 4B shows that the largest number of miRNAs were associated with metastasis, and TGF-β signaling pathway was also identified in the KEGG enrichment analysis (Fig. 4C).

To identify which miRNA was involved in acidic pH-induced EMT process, three bioinformatic software including TargetScan, StarBase and miRDB were used to predict the potential miRNAs. Eleven candidates were highlighted based on the overlapping gene candidates in three databases and in the miRNA-Seq analysis (Fig. S4B). By comparing these candidates and the down-regulated miRNAs as revealed by our miRNA-seq, we shortlisted five overlapping miRNAs candidates, they were miR-193a-3p, miR-193b-3p, miR-29a-3p, miR-29b-3p and miR-7-5p (Fig. 4D). Further study showed that among these five miRNAs, only miR-7-5p expression was reduced in the NSCLC cells (A549 and H1975) after being cultured in the pH 6.6 acidic medium (Fig. 4E). Moreover, reversal of the acidic environment diminished these effects (Fig. S4C), suggesting that miR-7-5p is a potential molecule that is regulated by the acidic environment. Interestingly, we found that overexpression of miR-7-5p using a miR-7-5p mimic diminished the acidic pH-induced A549 cell migration and invasion, similar results were shown in H1975 cells (Fig. 4F). On the other hand, inhibition of miR-7-5p using a miR-7-5p inhibitor increased NSCLC (A549 and H1975) cell migration and invasion under neutral pH environment (pH 7.4, Fig. 4G). Thus, these data clearly demonstrate that the acidic environment (pH 6.6) reduced miR-7-5p expression, which underlies the acidic pH-induced lung cancer metastasis.

3.5. *TGF-β2 is a potential target of miR-7-5p*

Since under the acidic environment, expression of TGF-β2 was increased but that of miR-7-5p was reduced, we attempted to explore whether TGF-β2 was a direct target of miR-7-5p. Data from the RNA pull-down assay showed that compared with the anti-sense group, sense group was greatly elevated, suggesting that the RNA of TGF-β2 interacts with miR-7-5p (Fig. 5A). Next, the dual luciferase reporter gene assay further confirmed these results. The luciferase reporter vector recombinant plasmids pTGF-β2-Wt (wild-type TGF-β2 3′-UTR; WT) and pTGF-β2 (mutant-type TGF-β2 3′-UTR; MUT) were constructed based on the TGF-β2 mRNA 3′-UTR (Fig. 5B). The luciferase activity in the miR-7 mimic+3′-UTRWT group was decreased by approximately 55.2% compared to that in the miR-NC+3′-UTRWT group (Fig. 5C). However, when comparing with miR-7 mimic+3′-UTRWT group, the miR-7 mimic+3′-UTR mut1 group, miR-7 mimic+mut2 group and miR-7 mimic+mut1+2 group all exhibited significant increase in luciferase activities, which were increased from 44.8% to 61.7%, 86.2%, and 90.1%, respectively (Fig. 5C). Therefore, these results suggest that TGF-β2 might be a direct downstream target of miR-7-5p.

To further determine the relationship between TGF-β2 and miR-7-5p, Western blot and qRT-PCR analyses were used to examine whether the miR-7-5p mimic could reverse the acidic pH-induced TGF-β2 activation. As expected, overexpression of miR-7-5p diminished the acidic pH-induced TGF-β2 activation in NSCLC cells (A549 and H1975) (Fig. 5D and E). Moreover, inhibition of miR-7-5p in NSCLC cells (A549 and H1975) cultured in normal medium (pH 7.4) increased TGF-β2 activity, and miR-7 inhibitor together with anti-TGF-β2 treatment diminished the miR-7 inhibitor-activated TGF-β2/SMAD signaling pathway (Fig. 5F). More importantly, the mRNA level of *TGF-β2* in A549 cells that were cultured in acidic medium (pH6.6) was decreased by 7.9-fold after treating with miR-7-5p mimic ($P < 0.01$) (Supporting Information Fig. S5A); while miR-7-5p level was increased by only 1.7-fold after TGF-β2 was knock-down in these cells, and the difference did not reach statistical

with miR-NC or miR-7 mimic in pH 6.6 cultured-NSCLC cells (A549 and H1975), respectively. (G) Representative images of the migrated and invade cells after treating with miR-NC or miR-7 inhibitor in pH 7.4 cultured NSCLC cells (A549 and H1975), respectively. Data are shown as mean ± SD from three independent experiments. $^{**}P < 0.01$ *vs.* miR-NC-treated cells.

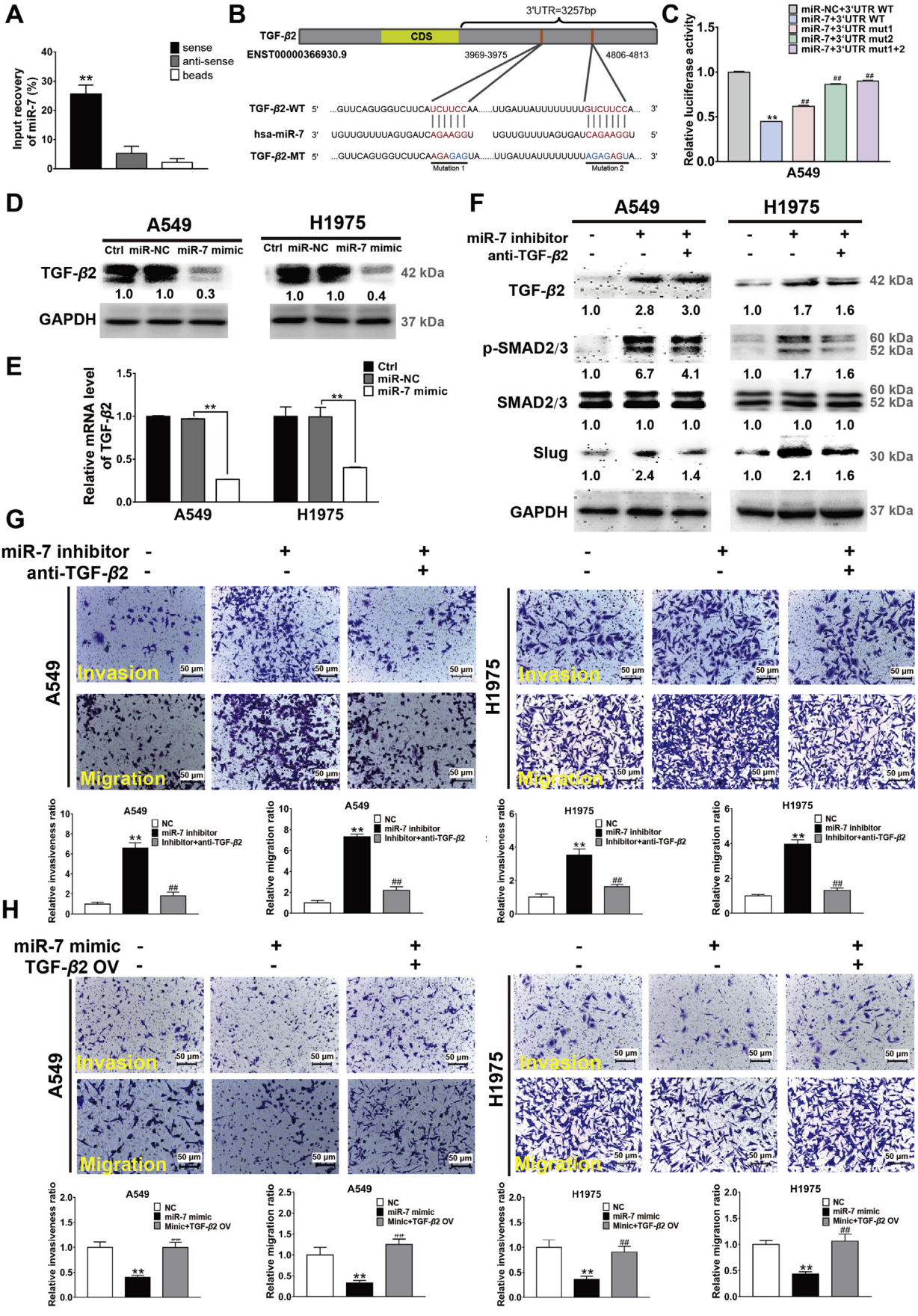
A
Input recovery of miR-7 (%)
sense
anti-sense
beads
B
3'UTR=3257bp
TGF-β2
CDS
ENST00000366930.9
3969-3975
4806-4813
TGF-β2-WT 5' ...GUUCAGUGGUCUUCAUCUUCCAA.....UUGAUUAUUUUUUUUGUCUUCCA... 3'
hsa-miR-7 3' UGUUGUUUUAGUGAUCAGAAGGU UGUUGUUUUAGUGAUCAGAAGGU 5'
TGF-β2-MT 5' ...GUUCAGUGGUCUUCAAGAGAGUA.....UUGAUUAUUUUUUUUAGAGAGUA... 3'
Mutation 1
Mutation 2
C
miR-NC+3'UTR WT
miR-7+3'UTR WT
miR-7+3'UTR mut1
miR-7+3'UTR mut2
miR-7+3'UTR mut1+2
Relative luciferase activity
A549
D
A549
H1975
Ctrl miR-NC miR-7 mimic
TGF-β2
GAPDH
42 kDa
37 kDa
1.0 1.0 0.3
1.0 1.0 0.4
E
Relative mRNA level of TGF-β2
Ctrl
miR-NC
miR-7 mimic
A549
H1975
F
A549
H1975
miR-7 inhibitor
anti-TGF-β2
TGF-β2
p-SMAD2/3
SMAD2/3
Slug
GAPDH
42 kDa
60 kDa
52 kDa
30 kDa
37 kDa
1.0 2.8 3.0
1.0 1.7 1.6
1.0 6.7 4.1
1.0 1.7 1.6
1.0 1.0 1.0
1.0 1.0 1.0
1.0 2.4 1.4
1.0 2.1 1.6
G
miR-7 inhibitor
anti-TGF-β2
A549
H1975
Invasion
Migration
50 μm
H
A549
H1975
Relative invasiveness ratio
Relative migration ratio
NC
miR-7 inhibitor
Inhibitor+anti-TGF-β2
miR-7 mimic
TGF-β2 OV
Minic+TGF-β2 OV

significance (Fig. S5B). Therefore, the above results suggest that miR-7 is a direct upstream regulator of TGF-β2.

The effects of miR-7-5p/TGF-β2 axis on cell invasion and migration were then studied by culturing A549 and H1975 cells in medium with pH 7.4 for 48 h in the presence or absence of anti-TGF-β2 antibody or miR-7-5p inhibitor. miR-7 inhibitor enhanced invasion and migration of the cells in the absence of the neutralizing anti-TGF-β2 antibody; the enhanced cell invasion and migration were reduced by the anti-TGF-β2 antibody treatment (Fig. 5G). On the contrary, for the cells that were cultured in acidic medium (pH 6.6), miR-7-5p mimic reduced the cell invasion and migration in the absence of the neutralizing antibody, which were reversed by the anti-TGF-β2 antibody treatment (Fig. 5H). These data further suggest that miR-7-5p and TGF-β2 play an important role in the acidic pH-enhanced lung cancer cell invasion and migration.

3.6. *Overexpression of miR-7-5p reduces tumor metastasis in animal models*

Next, metastatic mouse model was used to confirm the contribution of miR-7-5p and TGF-β2 in tumor metastasis *in vivo*. miR-7-5p was overexpressed in A549 cells with the lentiviral transduction method. Supporting Information Fig. S6A shows the fluorescence of A549-Lv-NC and A549-Lv-miR-7 cells. These cells were then injected into the lateral tail vein of nude mice. Detailed experimental procedures and timeline were shown in Fig. 6A. Results show that the number of metastatic lung nodules was significantly reduced in the Lv-miR-7-5p group compared to that in the Lv-NC group ($P < 0.05$) (Fig. 6B and C); moreover, the tumor size in the Lv-miR-7-5p group was smaller than that in the Lv-NC group (Fig. 6D). Importantly, overexpression of miR-7-5p reduced the expression of TGF-β2 in the tumor tissues as demonstrated by Western blot (Fig. 6E) and IHC (Fig. 6F) analyses. Notably, no animal death was recorded in all the groups, and no significant differences in the body weight (Fig. S6B) and organ index (Fig. S6C) were found between these two groups of mice. Collectively, these results not only validate TGF-β2 is a direct target of miR-7-5p, but also illustrate their roles in regulating lung cancer metastasis *in vivo*.

3.7. *Lung cancer patients have reduced miR-7-5p expression and elevated levels of activated TGF-β2*

To suggest whether our *in vitro* and *in vivo* findings on miR-7-5p and TGF-β2 in lung cancer had any clinical significance, we examined the expressions of TGF-β2 and miR-7-5p with the human LUAD and LUSC tissue microarrays, and their correlations with patients' survival. In IHC study, we found that TGF-β2 immunoreactivity was detected predominantly in the cytoplasm of carcinoma cells as clusters of yellow-brown granules; in contrast, weak or negative TGF-β2 staining was observed in adjacent normal lung epithelial cells and in the surrounding mesenchymal cells; TGF-β2 was significantly activated in tumor tissues but not in adjacent normal tissues from patients with LUAD ($P < 0.001$) and LUSC ($P < 0.001$), respectively (Fig. 6G). Moreover, high expression of TGF-β2 was inversely correlated with the survival of LUAD patients ($P = 0.0068$, $P < 0.01$) and LUSC patients ($P = 0.0235$, $P < 0.05$), respectively (Fig. 6I). No correlation was detected between TGF-β2 expression and the other standard clinicopathological variables, such as sex, pathological T stage, N stage (Table S1) and TNM stage (Fig. S6D).

The ISH analysis results does not show any correlations between miR-7 expression and the standard clinicopathological variables, such as sex, pathological T stage, N stage (Table S2) and TNM stage (Fig. S6E). However, the levels of miR-7 were lower in the tumor tissues than in adjacent normal tissues in the clinical samples of LUAD and LUSC, respectively (Fig. 6H). The reduced expression of miR-7 had a significant correlation with the survival of LUAD patients ($P = 0.0162$, $P < 0.05$) and LUSC patients ($P = 0.0396$, $P < 0.05$), respectively (Fig. 6J). Furthermore, the expressions of miR-7-5p and TGF-β2 in the tumor tissues were inversely correlated in both the LUAD patients ($P < 0.001$) and LUSC patients ($P < 0.001$, Fig. 6K).

These findings are consistent with our *in vivo* and *in vitro* data; and also demonstrate the correlation between miR-7-5p and TGF-β2 with patients' survival, which implying a pathological role of miR-7-5p and TGF-β2 in lung cancer.

4. Discussion

The changes of acidic TME could induce invasion, proliferation, and immune response, as well as tumor dormancy[34]. Acidosis is recognized as a chronic and harsh TME that educates malignant cells to thrive and metastasize. Although overwhelming evidence supports an acidic environment as a driver or ubiquitous hallmark of cancer progression, the unrevealed core mechanisms underlying the direct effect of acidification on tumorigenesis have hindered the discovery of novel therapeutic targets and clinical therapy. Here, our study reveals a predominate, direct and clear molecular signaling pathway responsible for tumor metastasis induced by acidic TME. The most significant and novel aspect of our work is that we are the first to reveal that acidic TME-induced lung cancer metastasis *via* inhibition of miR-7-5p. TGF-β2 is a direct target of

Figure 5 TGF-β2 is a direct target of miR-7-5p. (A) RNA pull-down assay was conducted using biotin-labeled T7 probe, and the miR-7-5p expression in the precipitate was measured by using qRT-PCR. An antisense T7 probe was used as its corresponding control. Beads was regarded as a negative control. (B) Potential miR-7-5p binding sequences in the 3′-UTR of TGF-β2 mRNAs were predicted *via* the TargetScan database. (C) The relative luciferase activity was analyzed after transfection of the described reporter plasmids (miR-7-3′-UTR) or mock reporter plasmid into A549 cells. *Firefly* luciferase activity was normalized to *Renilla* luciferase activity. $^{**}P < 0.01$ *vs.* miR-NC-3′-UTR WT, $^{\#\#}P < 0.01$ *vs.* miR-7-3′-UTR WT. The protein (D) and mRNA (E) levels of TGF-β2 after treated with miR-NC and the miR-7 mimic in pH6.6-treated A549 and H1975 cells were examined by using Western blot and qRT-PCR analyses, respectively. $^{**}P < 0.01$ *vs.* miR-NC-treated cells. (F) The protein levels of TGF-β2, SMAD2, p-SMAD2, SMAD3, p-SMAD3 and slug in pH6.6 cultured-NSCLC cells (A549 and H1975) after treated with miR-7 inhibitor and/or anti-TGF-β2 antibody were determined by using Western blot analysis. (G) Representative images of the migrated and invade cells after treating with miR-7 inhibitor and/or anti-TGF-β2 antibody in pH 7.4 cultured-NSCLC cells (A549 and H1975), respectively. $^{**}P < 0.01$ *vs.* miR-NC-treated cells; $^{\#\#}P < 0.01$ *vs.* miR-7 inhibitor-treated cells. (H) Representative images of the migrated and invade cells after treating with miR-7 mimic and/or TGF-β2 OV in pH 6.6 cultured-NSCLC cells (A549 and H1975), respectively. $^{**}P < 0.01$ *vs.* miR-NC-treated cells; $^{\#\#}P < 0.01$ *vs.* miR-7 mimic-treated cells. Data are shown as mean ± SD from three independent experiments.

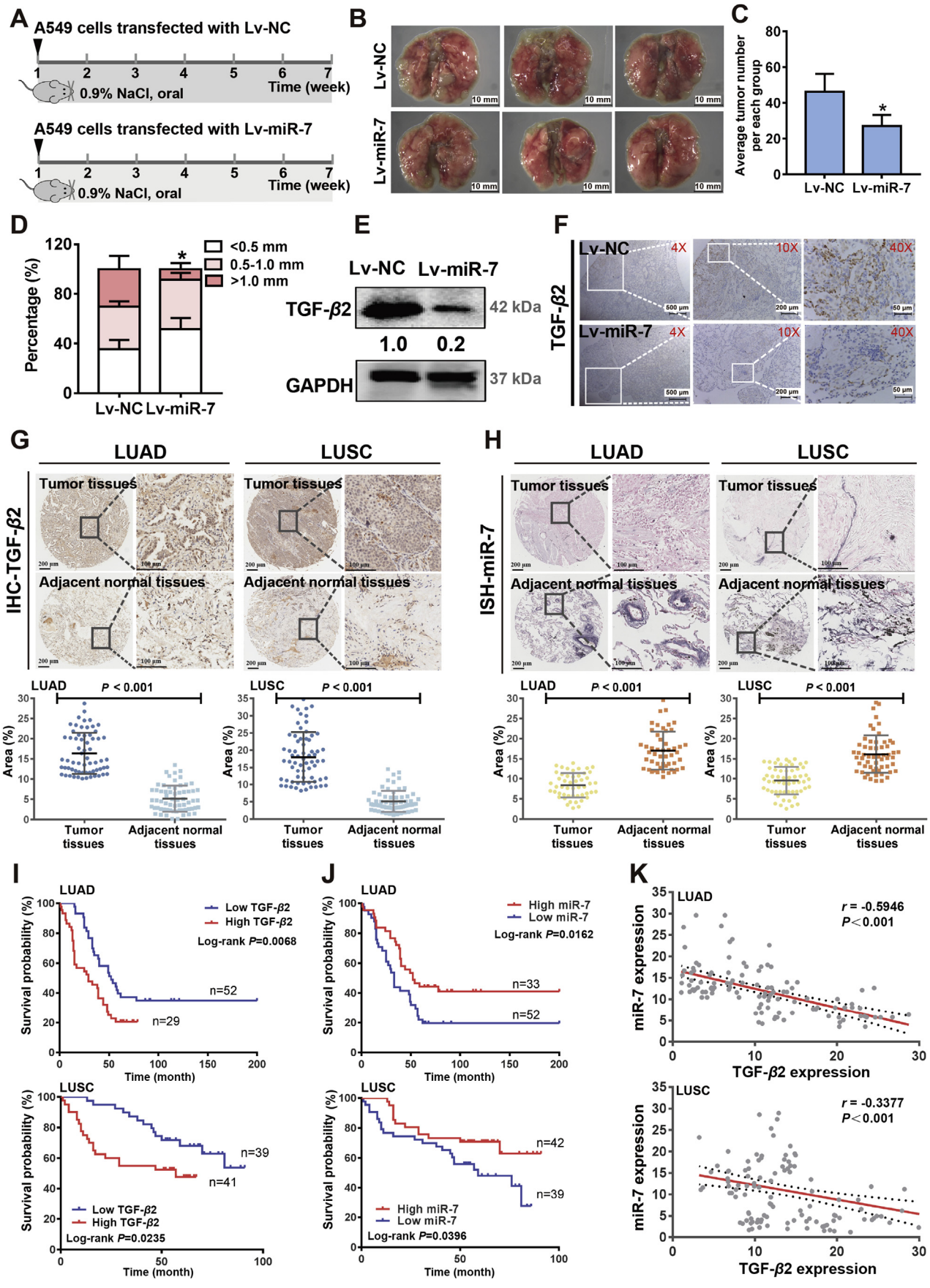
A
A549 cells transfected with Lv-NC
1 2 3 4 5 6 7
Time (week)
0.9% NaCl, oral
A549 cells transfected with Lv-miR-7
1 2 3 4 5 6 7
Time (week)
0.9% NaCl, oral
B
Lv-NC
Lv-miR-7
10 mm
C
Average tumor number per each group
80
60
40
20
0
*
Lv-NC Lv-miR-7
D
Percentage (%)
120
80
40
0
*
<0.5 mm
0.5-1.0 mm
>1.0 mm
Lv-NC Lv-miR-7
E
Lv-NC Lv-miR-7
TGF-β2
42 kDa
1.0 0.2
GAPDH
37 kDa
F
TGF-β2
Lv-NC
Lv-miR-7
4X
10X
40X
500 μm
200 μm
50 μm
G
LUAD
LUSC
IHC-TGF-β2
Tumor tissues
Adjacent normal tissues
200 μm
100 μm
LUAD P < 0.001
LUSC P < 0.001
Area (%)
Tumor tissues
Adjacent normal tissues
H
LUAD
LUSC
ISH-miR-7
Tumor tissues
Adjacent normal tissues
200 μm
100 μm
LUAD P < 0.001
LUSC P < 0.001
Area (%)
Tumor tissues
Adjacent normal tissues
I
LUAD
Survival probability (%)
Low TGF-β2
High TGF-β2
Log-rank P=0.0068
n=52
n=29
Time (month)
LUSC
Survival probability (%)
n=39
n=41
Low TGF-β2
High TGF-β2
Log-rank P=0.0235
Time (month)
J
LUAD
Survival probability (%)
High miR-7
Low miR-7
Log-rank P=0.0162
n=33
n=52
Time (month)
LUSC
Survival probability (%)
n=42
n=39
High miR-7
Low miR-7
Log-rank P=0.0396
Time (month)
K
LUAD
r = -0.5946
P<0.001
miR-7 expression
TGF-β2 expression
LUSC
r = -0.3377
P<0.001
miR-7 expression
TGF-β2 expression

miR-7-5p. Reduced miR-7-5p expression will enhance TGF-β2 expression, which in turn increases lung cancer metastasis.

Our works deepen our understanding on acidosis-induced tumorigenesis. (i) Firstly, as indicated previously[10], an acidic extracellular pH keeps the intercellular pH slightly alkaline at 7.12−7.65, but the variation in the pH of subcellular organelles in the alkaline cytoplasm was uncharacterized. Previous studies suggest that each intercellular compartment exhibits a different basal pH value, for example, pH 4.7 in lysosomes, pH 8.0 in mitochondria, and pH 5.8 in the nucleus[35]. Another study showed that the nucleus is alkaline, which is similar to the cytoplasm[36]. The inverse pH gradients in the nucleus and cytoplasm imply that the pH_i is not integral and uniform and that each subcellular organelle may prefer and exhibit different pH conditions to adapt to the new acidic homeostasis. (ii) Secondly, proteomic analysis has revealed that acidosis, either acute or chronic treatment, markedly reduces the levels of RNA-processing proteins in the nucleus rather than the other components in the cytoplasm (Fig. 4A). Our findings suggest that proteins that are involved in RNA synthesis and maturation are sensitive to the acidic environments, which not only supports the discovery of novel acidosis-dependent miRNA regulators, but also provides insight into the direct effects of acidification in carcinogenesis. (iii) Thirdly, to date, numerous mechanisms indicate that acidosis-induced tumorigenesis involves a diverse array of factors[3], but whether a slight change in pH can alter the translation or transcription of the functional regulators is unknown. What is the direct linkage between pH and signal transduction that is independent of other mediators? Our data show that the miR-7-5p/TGF-β2 axis was significantly altered during acidification.

A previous study shows that miR-7 expression is negatively correlated with TGF-β2 expression[38]. In this study, our data reveal that miR-7-5p is a novel upstream posttranscriptional factor and have identified its precise binding site with TGF-β2 in the 3′-UTR region. We clearly reveal that miR-7-5p directly bound to two "seed regions" of AGAAGG and CAGAAGG nucleotides at positions 3969−3975 and 4806−4813, respectively, in the 3′-UTR of TGF-β2 (Fig. 5B), while this recognized affinity is attenuated when these binding sites are mutated (Fig. 5C). Meanwhile, we also notice that unlike mutation 2, mutation 1 allows some recognitions and binding of miR-7-5p to the TGF-β2 possibly because in mutation 1, only three nucleotides are mutated (AGG to GAG), and this change might be insufficient to impede the complementary recognition of miR-7-5p to TGF-β2. When both sites are mutated (both mutations 1 and 2), the binding ability of miR-7-5p to TGF-β2 is similar to that of mutation 2, suggesting that the site in mutation 2 (4806−4813) is the main recognition domain in miR-7-5p for TGF-β2. Although our data also show that knockdown of TGF-β2 increases miR-7-5p level by 1.7-fold, the difference does not reach statistical significance, suggesting that a reciprocal regulatory manner between miR-7-5p and TGF-β2 is very unlikely. Indeed, the identification of the main recognition domain in miR-7-5p for TGF-β2 has demonstrated that miR-7-5p is the predominant upstream regulator of TGF-β2 (Supporting Information Fig. S5A and S5B).

TGF-β is a multifunctional regulatory cytokine that exerts tumor-suppressive effects in normal cells, but it also has pro-tumorigenic effects in cancer[37]. Interestingly, here, we found that the miR-7/TGF-β axis exhibits dual roles in normal fibroblasts and tumor cells. Elevated miR-7 expression significantly suppresses the mRNA and protein levels of *TGF-β2* in NSCLC cells (A549 and H1975) (Fig. 5D and E), but attenuating the cytotoxicity or antiproliferative activity of acidosis in MRC-5 pulmonary fibroblasts (Fig. S5C and S5D). More interestingly, our data also demonstrate that miR-7-targeted acidosis-optimal treatment inhibits the metastasis of EGFR-mutated cancer cells. Our data reveal that miR-7 deprivation not only sustains the migration and invasion of A549 cells but also the H1975 cells (Fig. 4G) which harbor L858R and T790M mutations that lead to the development of the resistance to EGFR inhibitors. Our data suggest that miRNA-7-targeted acidic TME-optimized therapy may be a novel EGFR-targeted therapeutic strategy for lung cancer treatment.

Besides, our study also proposes miR-7-5p as a novel reliable biomarker for acidic TME. Acidic TME biomarkers have been proposed, such as CA9, MCT4, and ATP6V0A1[9] which are abundantly expressed in the tumor tissues compared to adjacent normal tissues (Fig. 1D). However, the correlations between the survival rate and the expressions of CA9 and ATP6V0A1 are only existed in certain cancer types (Fig. 1A and Fig. S1A). Furthermore, neutralization of the acidic microenvironment markedly reduces the expressions of CA9 and MCT4 but not ATP6V0A1 and SLC9A1 in the animal models (Fig. 1E). These observations suggest that a more reliable and cancer-specific biomarker for the acidic TME has to be identified. By characterizing the landscape of gene and protein alterations during acidification, we found that miR-7-5p and TGF-β2 play a dominant role in acidosis-triggered metastasis, and their expressions are strongly correlated with the survival rates in both LUAD and LUSC (Fig. 6I and J). Furthermore, we found that miR-7-5p is a sensitive biomarker that responses to acidosis before other biomarkers do.

By integrating multi-omics analysis, *in vivo* data from six chemical-induced and transgenic animal models, as well as examination with clinical human cancer samples, we have provided the following novel findings: (i) This is the first evidence illustrates a direct correlation between extracellular acidification and tumorigenesis, and the process of pH-triggered protein degradation has suggested a novel angle to understand acidosis-associated tumorigenesis; (ii) Our works suggest that miRNA-synthesis process would be a novel network approach for the discovery of therapeutic targets for TME-adjusting cancer therapy; (iii) This

Figure 6 miR-7-5p and TGF-β2 are negatively correlated. (A) Timeline of the animal study. Mice were randomly divided into 2 groups: Lv-NC and Lv-miR-7. (B) Representative photographs showing the tumors in the lung tissues harvested from mice in Lv-NC and Lv-miR-7-5p groups. (C) Tumor number. $^*P < 0.05$ *vs.* Lv-NC group. (D) Tumor size. (E) The protein levels of TGF-β2 in Lv-NC and Lv-miR-7-5p groups were examined by using Western blot analysis. (F) The expression of TGF-β2 in tumor tissues were stained by IHC assay. (G) The expression of TGF-β2 in tumor tissues and adjacent normal tissues of clinical LUAD and LUSC patients were stained by IHC assay, $n = 184$. (H) The expression of miR-7 in tumor tissues and adjacent normal tissues of clinical LUAD and LUSC patients were examined by ISH assay, $n = 184$. (I) Survival curves of TGF-β2 in clinical LUAD and LUSC patients, respectively. (J) Survival curves of miR-7-5p in clinical LUAD and LUSC patients, respectively. (K) Negative correlation between TGF-β2 and miR-7-5p in clinical LUAD and LUSC patients. For the *in vivo* study, data are presented as mean ± SD, $n = 6$, $^*P < 0.05$ *vs.* Lv-NC treated mice.

study has provided the first and comprehensive clue for illustrating organic and phenotypic contextual of TME in solid tumors, and also provides solid scientific evidences to explain why the efficacies of the TME-targeted therapies in different cancer types are different. Last but not least, (iv) Our interesting findings showing the potent anti-metastatic effects of miR-7 in EGFR inhibitor-resistant H1975 cells suggests that miR-7-targeted therapy may be a novel alternative strategy to overcome the drug resistance to EGFR inhibitors in lung cancer.

Due to the limitation of novel, specific and sensitive markers for acidosis, the efficacy of acidosis-targeting therapy is still controversial and in-depth investigation is needed. Our findings have suggested novel and pragmatic strategies for the development of TME-targeting therapy, which are developing miR-7-aptamers and miR-7-agonist to reverse the acidic environment in TME, our findings can greatly enhance the efficacy of acidosis-targeting therapy.

5. Conclusions

Our data show that by significantly suppressed miR-7, acidic tumor microenvironment transcriptionally activated TGF-β2, which subsequently sustained the metastatic potential of both wild-type and EGFR-mutated lung cancer. The miR-7/TGF-β axis plays a critical role in the acidic pH-induced lung cancer metastasis. miR-7 is not only a novel reliable acidic TME biomarker, it also represents a novel therapeutic target for lung cancer treatment.

Data availability

RNA-Seq and miRNA-Seq (Submission No. SUB6634909) are available in Sequence Read Archive (SRA) database (Project No. PRJNA593422); Proteomics (PXD016524) are available in Proteomics identifications database.

Acknowledgments

This work was supported by the projects of National Natural Science Foundation of China (81874367 and 82074019), Guangdong Key Laboratory for Translational Cancer research of Chinese Medicine (2018B030322011, China), Natural Science Foundation for Distinguished Young Scholars of Guangdong Province, China (2017A030306033), Guangdong Province Universities and Colleges Pearl River Scholar Funded Scheme (2016, China), Project of Educational Commission of Guangdong Province of China (2016KTSCX012) and Pearl River Nova Program of Guangzhou, China (201710010108).

Author contributions

Tao Su and Suchao Huang performed the majority experiments. Yanmin Zhang, Yajuan Guo, Shuwei Zhang, Jiaji Guan, Mingjing Meng, Linxin Liu, Caiyan Wang, Zhiying Huang, Qiuju Huang and Ying Wang participated in some experiments. Tao Su and Linlin Lu interpreted the data and drafted the manuscript. Dihua Yu, Hiu-Yee Kwan, Elaine Lai-Han Leung and Ming Hu participated in the study design and provided some suggestions. Tao Su, Zhongqiu Liu and Linlin Lu supervised the study, reviewed the original data and finalized the manuscript. All authors have read and approved the final manuscript.

Conflicts of interest

The authors declare that they have no competing interests.

Appendix A. Supporting information

Supporting data to this article can be found online at https://doi.org/10.1016/j.apsb.2021.06.009.

References

1. Zhuang X, Zhang H, Hu G. Cancer and microenvironment plasticity: double-edged swords in metastasis. *Trends Pharmacol Sci* 2019;**40**:419–29.
2. Pichler M, Calin GA. MicroRNAs in cancer: from developmental genes in worms to their clinical application in patients. *Br J Cancer* 2015;**113**:569–73.
3. Corbet C, Feron O. Tumour acidosis: from the passenger to the driver's seat. *Nat Rev Cancer* 2017;**17**:577–93.
4. Gillies RJ, Verduzco D, Gatenby RA. Evolutionary dynamics of carcinogenesis and why targeted therapy does not work. *Nat Rev Cancer* 2012;**12**:487–93.
5. Marino ML, Pellegrini P, Di Lernia G, Djavaheri-Mergny M, Brnjic S, Zhang XN, et al. Autophagy is a protective mechanism for human melanoma cells under acidic stress. *J Biol Chem* 2012;**287**:30664–76.
6. Johnston RJ, Su LJ, Pinckney J, Critton D, Boyer E, Krishnakumar A, et al. VISTA is an acidic pH-selective ligand for PSGL-1. *Nature* 2019;**574**:565–70.
7. Peppicelli S, Andreucci E, Ruzzolini J, Laurenzana A, Margheri F, Fibbi G, et al. The acidic microenvironment as a possible niche of dormant tumor cells. *Cell Mol Life Sci* 2017;**74**:2761–71.
8. Pillai SR, Damaghi M, Marunaka Y, Spugnini EP, Fais S, Gillies RJ. Causes, consequences, and therapy of tumors acidosis. *Cancer Metast Rev* 2019;**38**:205–22.
9. Neri D, Supuran CT. Interfering with pH regulation in tumours as a therapeutic strategy. *Nat Rev Drug Discov* 2011;**10**:767–77.
10. Cardone RA, Casavola V, Reshkin SJ. The role of disturbed pH dynamics and the Na^+/H^+ exchanger in metastasis. *Nat Rev Cancer* 2005;**5**:786–95.
11. Damaghi M, Tafreshi NK, Lloyd MC, Sprung R, Estrella V, Wojtkowiak JW, et al. Chronic acidosis in the tumour microenvironment selects for overexpression of LAMP2 in the plasma membrane. *Nat Commun* 2015;**6**:8752–64.
12. Rosko AE, McColl KS, Zhong F, Ryder CB, Chang MJ, Sattar A, et al. Acidosis sensing receptor GPR65 correlates with anti-apoptotic Bcl-2 family member expression in CLL cells: potential implications for the CLL microenvironment. *J Leuk (Los Angel)* 2014;**2**:160–74.
13. Wojtkowiak JW, Rothberg JM, Kumar V, Schramm KJ, Haller E, Proemsey JB, et al. Chronic autophagy is a cellular adaptation to tumor acidic pH microenvironments. *Cancer Res* 2012;**72**:3938–47.
14. Tian XP, Wang CY, Jin XH, Li M, Wang FW, Huang WJ, et al. Acidic microenvironment up-regulates exosomal miR-21 and miR-10b in early-stage hepatocellular carcinoma to promote cancer cell proliferation and metastasis. *Theranostics* 2019;**9**:1965–79.
15. Shang P, Gao R, Zhu Y, Zhang X, Wang Y, Guo M, et al. VEGFR2-targeted antibody fused with IFN α mut regulates the tumor microenvironment of colorectal cancer and exhibits potent anti-tumor and anti-metastasis activity. *Acta Pharm Sin B* 2021;**11**:420–33.
16. Su T, Yang X, Deng JH, Huang QJ, Huang SC, Zhang YM, et al. Evodiamine, a novel NOTCH3 methylation stimulator, significantly

suppresses lung carcinogenesis *in vitro* and *in vivo*. *Front Pharmacol* 2018;**9**:434−46.
17. Su T, Bai JX, Chen YJ, Wang XN, Fu XQ, Li T, et al. An ethanolic extract of Ampelopsis Radix exerts anti-colorectal cancer effects and potently inhibits STAT3 signaling *in vitro*. *Front Pharmacol* 2017;**8**:227−36.
18. Chen L, Chen L, Qin Z, Lei J, Ye S, Zeng K, et al. Upregulation of miR-489-3p and miR-630 inhibits oxaliplatin uptake in renal cell carcinoma by targeting OCT2. *Acta Pharm Sin B* 2019;**9**:1008−20.
19. Lv S, Ji L, Chen B, Liu S, Lei C, Liu X, et al. Histone methyltransferase KMT2D sustains prostate carcinogenesis and metastasis *via* epigenetically activating LIFR and KLF4. *Oncogene* 2018;**37**:1354−68.
20. Li B, Dewey CN. RSEM: accurate transcript quantification from RNA-Seq data with or without a reference genome. *BMC Bioinf* 2011;**12**:323−38.
21. Huang da W, Sherman BT, Lempicki RA. Systematic and integrative analysis of large gene lists using DAVID bioinformatics resources. *Nat Protoc* 2009;**4**:44−57.
22. Subramanian A, Tamayo P, Mootha VK, Mukherjee S, Ebert BL, Gillette MA, et al. Gene set enrichment analysis: a knowledge-based approach for interpreting genome-wide expression profiles. *Proc Natl Acad Sci U S A* 2005;**102**:15545−50.
23. Shen Y, Zhang F, Li FP, Jiang XH, Yang YH, Li XL, et al. Loss-of-function mutations in QRICH2 cause male infertility with multiple morphological abnormalities of the sperm flagella. *Nat Commun* 2019;**10**:433−47.
24. Kato Y, Ozawa S, Miyamoto C, Maehata Y, Suzuki A, Maeda T, et al. Acidic extracellular microenvironment and cancer. *Cancer Cell Int* 2013;**13**:89−96.
25. De Milito A, Canese R, Marino ML, Borghi M, Iero M, Villa A, et al. pH-dependent antitumor activity of proton pump inhibitors against human melanoma is mediated by inhibition of tumor acidity. *Int J Cancer* 2010;**127**:207−19.
26. Huber AR, Tan DF, Sun J, Dean D, Wu TT, Zhou ZR. High expression of carbonic anhydrase IX is significantly associated with glandular lesions in gastroesophageal junction and with tumorigenesis markers BMI1, MCM4 and MCM7. *BMC Gastroenterol* 2015;**15**:180−8.
27. Smith AD, Truong M, Bristow R, Yip P, Milosevic MF, Joshua AM. The utility of serum CA9 for prognostication in prostate cancer. *Anticancer Res* 2016;**36**:4489−92.
28. Whitton B, Okamoto H, Packham G, Crabb SJ. Vacuolar ATPase as a potential therapeutic target and mediator of treatment resistance in cancer. *Cancer Med* 2018;**7**:3800−11.
29. Robey IF, Baggett BK, Kirkpatrick ND, Roe DJ, Dosescu J, Sloane BF, et al. Bicarbonate increases tumor pH and inhibits spontaneous metastases. *Cancer Res* 2009;**69**:2260−8.
30. Kondo A, Yamamoto S, Nakaki R, Shimamura T, Hamakubo T, Sakai J, et al. Extracellular acidic pH activates the sterol regulatory element-binding protein 2 to promote tumor progression. *Cell Rep* 2017;**18**:2228−42.
31. Chen C, Bai LP, Cao FQ, Wang SN, He HW, Song MC, et al. Targeting LIN28B reprograms tumor glucose metabolism and acidic microenvironment to suppress cancer stemness and metastasis. *Oncogene* 2019;**38**:4527−39.
32. Kubiczkova L, Sedlarikova L, Hajek R, Sevcikova S. TGF-beta an excellent servant but a bad master. *J Transl Med* 2012;**10**:183−206.
33. Derynck R, Zhang YE. Smad-dependent and Smad-independent pathways in TGF-beta family signalling. *Nature* 2003;**425**:577−84.
34. Hu WH, Zhang LC, Dong YT, Tian ZS, Chen YQ, Dong SW. Tumour dormancy in inflammatory microenvironment: a promising therapeutic strategy for cancer-related bone metastasis. *Cell Mol Life Sci* 2020;**77**:5149−69.
35. Hou H, Zhao Y, Li C, Wang M, Xu X, Jin Y. Single-cell pH imaging and detection for pH profiling and label-free rapid identification of cancer-cells. *Sci Rep* 2017;**7**:1759−66.
36. Masuda A, Oyamada M, Nagaoka T, Tateishi N, Takamatsu T. Regulation of cytosol-nucleus pH gradients by K^+/H^+ exchange mechanism in the nuclear envelope of neonatal rat astrocytes. *Brain Res* 1998;**807**:70−7.
37. Riemann A, Reime S, Thews O. Acidic extracellular environment affects miRNA expression in tumors *in vitro* and *in vivo*. *Int J Cancer* 2019;**144**:1609−18.
38. Shih JC, Lin HH, Hsiao AC, Su YT, Tsai S, Chien CL, et al. Unveiling the role of microRNA-7 in linking TGF-beta-Smad-mediated epithelial-mesenchymal transition with negative regulation of trophoblast invasion. *FASEB J* 2019;**33**:6281−95.